Improvement on RCS reduction using flat lossy focusing reflectors

Cheng-Yuan Chin* **and Christina F. Jou**

Department of Electrical Engineering, National Chiao-Tung University, Hsinchu, Taiwan

*paladinchin@gmail.com

Abstract: In this paper, we propose a planar non-periodic subwavelength resistive grating (SWRG). The phase front of the scattered fields can be completely manipulated through non-periodic design of the grating while high absorptivity is preserved. The SWRG has an interesting property similar to a resistive concave reflecting lens. Scattered wave is focused in the near-field region, and spread out in the far-field. This feature of non-periodic resistive grating can improve the original radar cross section (RCS) reduction up to 22.86 dB in the boresight direction comparing to the periodic counterpart. Non-periodic design of SWRG could have a substantial impact on stealth technology, aerospace engineering, and microwave anechoic chamber.

OCIS codes: (010.1030) Absorption; (050.6624) Subwavelength structures; (350.4010) Microwaves.

References and links

1. W. W. Salisbury, "Absorbent body of electromagnetic waves" (1952).
2. R. Fante and M. McCormack, "Reflection properties of the salisbury screen," IEEE Trans. Antennas Propag. **36**, 1443–1454 (1988).
3. F. Costa, A. Monorchio, and G. Manara, "Analysis and design of ultra thin electromagnetic absorbers comprising resistively loaded high impedance surfaces," IEEE Trans. Antennas Propag. **58**, 1551–1558 (2010).
4. F. C. Seman, R. Cahill, and V. Fusco, "Performance enhancement of salisbury screen absorber using a resistively loaded high impedance ground plane," in *Proc. of the 4th European Conference on Antennas and Propagation (EUCAP 2010)* (Barcelona, Spain, 2010), pp. 1–5.
5. F. C. Seman, R. Cahill, V. Fusco, and G. Goussetis, "Design of a salisbury screen absorber using frequency selective surfaces to improve bandwidth and angular stability performance," IET Microwaves Antennas Propag. **5**, 149–156 (2011).
6. H. B. Zhang, P. H. Zhou, L. W. Deng, J. L. Xie, D. F. Liang, and L. J. Deng, "Frequency-dispersive resistance of high impedance surface absorber with trapezoid-coupling pattern," J. Appl. Phys. **112**, 014106 (2012).
7. Y.-Q. Pang, Y.-J. Zhou, and J. Wang, "Equivalent circuit method analysis of the influence of frequency selective surface resistance on the frequency response of metamaterial absorbers," J. Appl. Phys. **110**, 023704 (2011).
8. L. K. Sun, H. F. Cheng, Y. J. Zhou, and J. Wang, "Broadband metamaterial absorber based on coupling resistive frequency selective surface," Opt. Express **20**, 4675–4680 (2012).
9. W. Choi, J. Shin, T. Song, J. Kim, W. Lee, Y. Joo, and C.-G. Kim, "Design of thin circuit-analogue multilayer absorber and application to leading edge of wing structure," Electron. Lett. **49**, 216–217 (2013).
10. J.-B. Kim and J.-H. Byun, "Salisbury screen absorbers of dielectric lossy sheets of carbon nanocomposite laminates," IEEE Trans. Electromagn. Compat. **54**, 37–42 (2012).
11. T. B. A. Senior, "Approximate boundary conditions," IEEE Trans. Antennas Propag. **29**, 826–829 (1981).
12. M. A. Leontovich, *Investigations on Radiowave Propagation, Part II* (Academy of Sciences, 1948).
13. T. B. A. Senior, "Impedance boundary conditions for imperfectly conducting surfaces," Appl. Sci. Res., Sect. B **8**, 418–436 (1960).
14. R.-B. Hwang, "Scattering characteristics of two-dimensionally periodic impedance surface," IEEE Trans. Antennas Propag. **48**, 1521–1527 (2000).

#198658 - $15.00 USD Received 1 Oct 2013; revised 12 Dec 2013; accepted 12 Dec 2013; published 23 Dec 2013

15. R.-B. Hwang, "Periodic impedance surface," in *Periodic Structures: Mode-Matching Approach and Applications in Electromagnetic Engineering*, 1st ed. (IEEE Press, 2012), chap. 6, pp. 277–280.
16. T. B. A. Senior, "Backscattering from resistive strips," IEEE Trans. Antennas Propag. **27**, 808–813 (1979).
17. T. Senior, "Combined resistive and conductive sheets," IEEE Trans. Antennas Propag. **33**, 577–579 (1985).
18. H. Bateman, *Electrical and Optical Wave Motion* (Cambridge University, 1955).
19. J. Volakis, Y.-C. Lin, and H. Anastassiu, "Te characterization of resistive strip gratings on a dielectric slab using a single edge-mode expansion," IEEE Trans. Antennas Propag. **42**, 205–212 (1994).
20. K. Whites and R. Mittra, "An equivalent boundary-condition model for lossy planar periodic structures at low frequencies," IEEE Trans. Antennas Propag. **44**, 1617–1629 (1996).
21. Y. Padooru, A. Yakovlev, C. S. R. Kaipa, G. Hanson, F. Medina, F. Mesa, and A. Glisson, "New absorbing boundary conditions and analytical model for multilayered mushroom-type metamaterials: Applications to wideband absorbers," IEEE Trans. Antennas Propag. **60**, 5727–5742 (2012).
22. A. Matsushima and T. Itakura, "Singular integral equation approach to plane wave diffraction by an infinite strip grating at oblique incidence," J. Electromagn. Waves Appl. **4**, 505–519 (1990).
23. T. Zinenko, A. Nosich, and Y. Okuno, "Plane wave scattering and absorption by resistive-strip and dielectric-strip periodic gratings," IEEE Trans. Antennas Propag. **46**, 1498–1505 (1998).
24. R. Hall and R. Mittra, "Scattering from a periodic array of resistive strips," IEEE Trans. Antennas Propag. **33**, 1009–1011 (1985).
25. R. Hall, R. Mittra, and K. Mitzner, "Scattering from finite thickness resistive strip gratings," IEEE Trans. Antennas Propag. **36**, 504–510 (1988).
26. M. G. Moharam and T. K. Gaylord, "Rigorous coupled-wave analysis of planar-grating diffraction," J. Opt. Soc. Am. **71**, 811–818 (1981).
27. M. G. Moharam, E. B. Grann, D. A. Pommet, and T. K. Gaylord, "Formulation for stable and efficient implementation of the rigorous coupled-wave analysis of binary gratings," J. Opt. Soc. Am. A **12**, 1068–1076 (1995).
28. D. Fattal, J. Li, Z. Peng, M. Fiorentino, and R. G. Beausoleil, "Flat dielectric grating reflectors with focusing abilities," Nat. Photonics **4**, 466–470 (2010).
29. F. Lu, F. G. Sedgwick, V. Karagodsky, C. Chase, and C. J. Chang-Hasnain, "Planar high-numerical-aperture low-loss focusing reflectors and lenses using subwavelength high contrast gratings," Opt. Express **18**, 12606–12614 (2010).

1. Introduction

From World War II, reducing the radar cross section (RCS) of a conducting body effectively have aroused much interest of engineers and scientists. For this reason, electromagnetic absorbers or radar absorbing materials (RAMs) have been explored against the threat of radar tracking system. One of the most popular techniques in RAM fabrication is based on Salisbury screens [1, 2]. Salisbury screen is a passive combination consisting of resistive sheet, dielectric substrate, and ground plane. The resistive sheet is mounted a quarter wavelegnth ($\lambda/4$) above the metallic ground plane using air substrate. Convenience of fabrication is the advantage of Salisbury screen.

Recently, many studies have dealt with the analysis of resistive gratings and received considerable attention. Resistive grating is constructed of periodic resistive sheet with specific pattern, such as printing frequency selective surface (FSS) with resistive ink [3–5], or printing FSS by silk screen printing technique through a photo etched frame with carbon black serum [6–8], and it possesses greater control of the grating's reflection characteristic. Besides planar configuration, non-planar applications were also demonstrated using resistive gratings. For instance, the multilayered absorber was bent and applied to the leading edge of a wing-shaped structure [9]. In fact, the lossy laminate is made of E-glass fiber/epoxy prepreg containing various kinds of carbon nano materials [10]. The electromagnetic property can be controlled by adding lossy nanofillers to the polymer matrix.

In order to compute scattering and other electromagnetic phenomena in the presence of resistive grating, it is necessary to introduce some simplification to make the problem tractable. Through the use of approximate boundary condition, the complexity and computational expenses of the analysis can be reduced [11]. Impedance and resistive boundary conditions are two remarkable examples. Impedance boundary condition is obtained by considering a plane

#198658 - $15.00 USD Received 1 Oct 2013; revised 12 Dec 2013; accepted 12 Dec 2013; published 23 Dec 2013

wave incident on a half plane [12–15], and it is assumed impenetrable. However, the resistive boundary condition is closely related to impedance boundary condition but has partial transparency [16, 17]. The idealized resistive sheet is infinitesimally thin so that the tangential electric fields are the same on both sides. Since it supports electric current at the surface, a discontinuity, referred to as a jump condition, for the tangential magnetic field components across the surface is originally proposed by Levi-Civita [18].

Using resistive boundary condition with a single edge-mode expansion for the strip current, a closed-form solution was derived for the TE mode scattering by a resistive strip array on a dielectric layer [19]. The solution was based on the assumption of small-width strips. Recently, an equivalent anisotropic resistive boundary condition (ARBC) was developed by Whites and Mittra [20]. This ARBC model can be used for infinite or finite periodic objects provided that the structure has rotational symmetry and sufficiently large surface resistance. A more complicated structure in the form of multilayered mushroom-type high impedance surface has been presented and characterized by a simple analytical model [21]. It is a combination of metallic wire medium and resistive patch arrays. This model gives accurate results when the slit between adjacent mushroom structures is much smaller than the periodicity for small and moderate values of surface resistance.

Many different formulations have been considered for analytical solutions to the problem of resistive gratings, and the use of integral equations and the spectral-Galerkin method are most familiar.

The key processes of the integral equation approach with singular kernel functions are to extract the logarithmic factor of the kernel function, and then using a group of orthogonal eigenfunctions of the singular element as the basis and testing functions in a moment procedure. This is a sophisticated version of traditional moment method, which is regarded as a regularization procedure, since the resultant set of linear algebraic equations is in the form of Fredholm second kind [22, 23].

The spectral-Galerkin method is another approach which has been harnessed successfully to periodic structures with zero thickness for both perfectly conducting and resistive surfaces. In the spectral domain, the convolution form of the integral equation for the scattered field reduces to product form by Fourier transformation. The unknown induced currents on the surface are expanded in a set of basis functions, and the matrix equation with expansion coefficients are then solved by moment method techniques [24, 25].

However, the above methods intend to solve the problem where the unit cell consists of only one kind of resistive strip. If there are more resistive strips having different resistances inside the unit cell, a reformulation process is needed according to the unit cell geometry and the total number of resistive strips. To address the issue, an approach enlightened by rigorous coupled wave analysis (RCWA) is presented in this paper, where Fourier expansion of inhomogeneous admittance function is used in order to synchronize with the Floquet mode matching analysis.

The paper is organized as follows. Section 2 provides the general formulation of wave scattering by a two-dimensional resistive grating. The concept of Fourier expansion is involved in the resistive boundary condition. Section 3 describes the configuration of the proposed SWRG. A detailed design procedure based on the unit cell analysis using RCWA is explained in Section 4. In Section 5, we conduct a full-wave simulation of the entire grating to verify the effectiveness of the non-periodic design concept. Section 6 summarizes the conclusions.

2. Formulation

In this section, we calculate the reflection and transmission characteristics of a multilayered periodic structure packed in a rectangular array. The structure is formed by a two-dimensional resistive grating sandwiched in two different homogeneous dielectric layers, which is depicted

#198658 - $15.00 USD Received 1 Oct 2013; revised 12 Dec 2013; accepted 12 Dec 2013; published 23 Dec 2013

in Fig. 1. The numerical analysis is performed based on the resistive boundary condition (RBC). In the following, a time variation of the form $e^{j\omega t}$ is assumed and suppressed, and both transverse electric (TE) and transverse magnetic (TM) polarizations are considered.

As noted by Levi-Civita [18], the RBCs at the resistive surface are

$$\hat{z} \times \left[\underline{E}_t(z=0^+) - \underline{E}_t(z=0^-)\right] = 0 \tag{1}$$

$$\hat{z} \times \left[\underline{H}_t(z=0^+) - \underline{H}_t(z=0^-)\right] = \underline{J} \tag{2}$$

and

$$\hat{z} \times \left[\hat{z} \times \underline{E}_t(z=0^{\pm})\right] = -Z_s \cdot \underline{J} \tag{3}$$

where the "+" and "-" signs refer to surfaces just above or below the sheet. Equation (1) implies that the tangential electric fields near the sheet in medium 1 and 2 are continuous at $z = 0$, while (2) is analogous to Kirchhoff's current law as shown in Fig. 2. Substituting (2) into (3) gives

$$\underline{H}_t(z=0^-) - \underline{H}_t(z=0^+) = Y_s \cdot \left[\hat{z} \times \underline{E}_t(z=0^{\pm})\right] \tag{4}$$

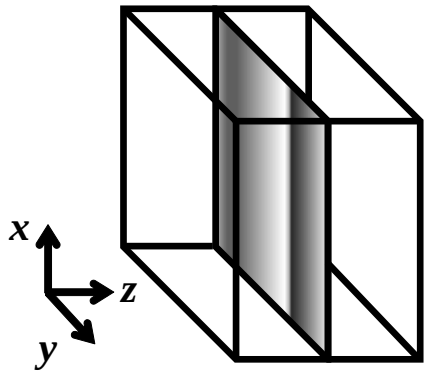

Fig. 1. Unit cell of resistive grating inserted in the middle of two distinct dielectric mediums.

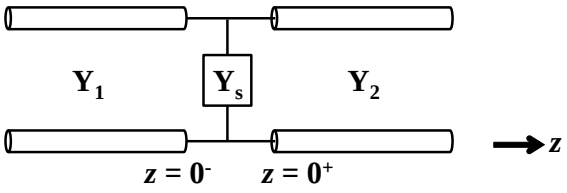

Fig. 2. Equivalent transmission line model for structure shown in Fig 1.

To simulate the electromagnetic properties of such grating, we employ the rigorous coupled wave analysis (RCWA), which was originally presented by Moharam and Gaylord [26, 27], with a few modification.

#198658 - $15.00 USD Received 1 Oct 2013; revised 12 Dec 2013; accepted 12 Dec 2013; published 23 Dec 2013

In accordance with Floquet's theorem, the tangential electric and magnetic fields within the homogeneous region are written as the Fourier expansion of spatial harmonics given by

$$\begin{aligned}\underline{E}_t &= \sum_{m=-\infty}^{\infty}\sum_{n=-\infty}^{\infty}\underline{e}_{tmn}(z)\cdot\exp(-j(k_{xm}x+k_{yn}y))\\ \underline{H}_t &= \sum_{m=-\infty}^{\infty}\sum_{n=-\infty}^{\infty}\underline{h}_{tmn}(z)\cdot\exp(-j(k_{xm}x+k_{yn}y))\end{aligned} \tag{5}$$

and

$$\begin{aligned}k_{xm} &= k\sin\theta\cos\phi+2\pi m/p_x\\ k_{yn} &= k\sin\theta\sin\phi+2\pi n/p_y\end{aligned} \tag{6}$$

where $\underline{e}_{tmn}(z)$ and $\underline{h}_{tmn}(z)$ represent the modal amplitudes of spatial harmonics for the electric and magnetic fields, respectively.

In the resistive grating layer, the sheet (located at $z=0$) is assumed to be infinitely thin and having periodic admittance distribution $Y_s(x,y)$. The period of grating along the x- and y- axes, are denoted by p_x and p_y, respectively. In (4), the Fourier component $Y_{m,n}$ of the admittance distribution $Y_s(x,y)$ is given by

$$Y_{m,n}=\frac{1}{p_xp_y}\int_0^{p_x}\int_0^{p_y}Y_s(x,y)\cdot\exp(j(\frac{2\pi m}{p_x}x+\frac{2\pi n}{p_y}y))dxdy \tag{7}$$

After substituting (5) and (7) into (1) and (4) and collecting the expanded Fourier components leads to

$$\begin{aligned}\underline{e}_{t1} &= \underline{e}_{t2}\\ \underline{h}_{t1}-\underline{h}_{t2} &= \mathbb{Y}_s\underline{e}_{t1}\end{aligned} \tag{8}$$

where

$$\underline{e}_t=\begin{bmatrix}-\underline{e}_y\\ \underline{e}_x\end{bmatrix},\ \underline{h}_t=\begin{bmatrix}\underline{h}_x\\ \underline{h}_y\end{bmatrix} \tag{9}$$

The electric and magnetic field components in (8) is further expressed in terms of eigenvectors in the homogeneous medium which gives

$$\begin{aligned}\mathbb{Q}_1(\underline{a}_1+\underline{b}_1) &= \mathbb{Q}_2(\underline{a}_2+\underline{b}_2)\\ \mathbb{Q}_1\mathbb{Y}_1(\underline{a}_1-\underline{b}_1)-\mathbb{Q}_2\mathbb{Y}_2(-\underline{a}_2+\underline{b}_2) &= \mathbb{Y}_s\mathbb{Q}_1(\underline{a}_1+\underline{b}_1)\end{aligned} \tag{10}$$

Parameters $\underline{a}$ and $\underline{b}$ are the incident and reflected wave amplitudes along the z-axis, while the subscript denotes in which medium the fields are. $\mathbb{Q}$ is a square matrix whose i-th column contains the eigenvector $\underline{q}_i$. $\mathbb{Y}_1$ (or $\mathbb{Y}_2$) is a diagonal matrix having the admittance of each eigenvector on its main entry. Specifically, $\mathbb{Y}_s$ is the admittance matrix of the resistive grating, and it will be a full matrix (a tensor) if the resistive grating is inhomogeneous.

Rearranging (10), the scattering matrix is derived as

#198658 - $15.00 USD Received 1 Oct 2013; revised 12 Dec 2013; accepted 12 Dec 2013; published 23 Dec 2013

$$
\begin{aligned}
\mathbb{S}_{11} &= (\mathbb{Q}_1^{-1}\mathbb{Q}_2\mathbb{Y}_2\mathbb{Q}_2^{-1}\mathbb{Q}_1 + \mathbb{Y}_1 + \mathbb{Q}_1^{-1}\mathbb{Y}_s\mathbb{Q}_1)^{-1}\cdot \\
&\qquad (-\mathbb{Q}_1^{-1}\mathbb{Q}_2\mathbb{Y}_2\mathbb{Q}_2^{-1}\mathbb{Q}_1 + \mathbb{Y}_1 - \mathbb{Q}_1^{-1}\mathbb{Y}_s\mathbb{Q}_1) \\
\mathbb{S}_{12} &= (\mathbb{Q}_1^{-1}\mathbb{Q}_2\mathbb{Y}_2\mathbb{Q}_2^{-1}\mathbb{Q}_1 + \mathbb{Y}_1 + \mathbb{Q}_1^{-1}\mathbb{Y}_s\mathbb{Q}_1)^{-1}\cdot \\
&\qquad (2\cdot\mathbb{Q}_1^{-1}\mathbb{Q}_2\mathbb{Y}_2) \\
\mathbb{S}_{21} &= (\mathbb{Q}_2^{-1}\mathbb{Q}_1\mathbb{Y}_1\mathbb{Q}_1^{-1}\mathbb{Q}_2 + \mathbb{Y}_2 + \mathbb{Q}_2^{-1}\mathbb{Y}_s\mathbb{Q}_2)^{-1}\cdot \\
&\qquad (2\cdot\mathbb{Q}_2^{-1}\mathbb{Q}_1\mathbb{Y}_1) \\
\mathbb{S}_{22} &= (\mathbb{Q}_2^{-1}\mathbb{Q}_1\mathbb{Y}_1\mathbb{Q}_1^{-1}\mathbb{Q}_2 + \mathbb{Y}_2 + \mathbb{Q}_2^{-1}\mathbb{Y}_s\mathbb{Q}_2)^{-1}\cdot \\
&\qquad (-\mathbb{Q}_2^{-1}\mathbb{Q}_1\mathbb{Y}_1\mathbb{Q}_1^{-1}\mathbb{Q}_2 + \mathbb{Y}_2 - \mathbb{Q}_2^{-1}\mathbb{Y}_s\mathbb{Q}_2)
\end{aligned}
\tag{11}
$$

The scattering matrices in the above equations fully describe the reflection and transmission properties of each eigenmode. And it is intuitive to find the analogy between the sandwiched resistive grating and two transmission lines with a shunt admittance in the middle, which is illustrated in Fig. 2. The scattering parameters of the latter case can be derived directly when each matrix on the right-hand side of (11) is replaced by a scalar.

$$
\begin{aligned}
S_{11} &= (Y_1 + Y_2 + Y_s)^{-1}(Y_1 - Y_2 - Y_s) \\
S_{12} &= (Y_1 + Y_2 + Y_s)^{-1}(2\cdot Y_2) \\
S_{21} &= (Y_1 + Y_2 + Y_s)^{-1}(2\cdot Y_1) \\
S_{22} &= (Y_1 + Y_2 + Y_s)^{-1}(-Y_1 + Y_2 - Y_s)
\end{aligned}
\tag{12}
$$

It is a meaningful way to interpret the resistive grating through the equivalent circuit model. When $Y_s = 0$, which means a shunt open circuit is between two transmission lines, no power is consumed by the grating; when $Y_s = \infty$, which means a shunt short circuit is between two transmission lines, the incident wave suffers a total reflection with 180° out of phase at the interface, and this case corresponds to a PEC sheet in reality.

3. Structure configuration

The purpose of this section is to construct a one-dimensional SWRG with non-periodic configuration and focusing ability, which operates at 10 GHz (λ_0 = 30 mm) under TM-polarized normal incidence. Although the numerical analysis of a two-dimensional periodic grating has been established, the equations cannot be applied to a one-dimensional case directly without modification. We define that p is the period along the x-axis, and the fields are independent of y ($\partial/\partial y = 0$). Thus, the waves can be individually decomposed into TE_z ($E_z = 0$) and TM_z ($H_z = 0$). Then the employed symbols are unified by setting $\phi = 0^\circ$, $p_x = p$, $p_y = \infty$, $\underline{e}_t = \underline{e}_x$, and $\underline{h}_t = \underline{h}_y$. Besides, the dimension of the admittance distribution also reduces to one. For example, if the surface resistance is 175 Ω/square, the admittance distribution $Y_s(x)$ of the unit cell shown in the inset of Fig. 3 can be defined as

$$
\begin{aligned}
Y_s(x) &= \frac{1}{175}, \quad -\frac{w}{2} \leqslant x \leqslant \frac{w}{2} \\
&= 0, \qquad\qquad \textit{otherwise}
\end{aligned}
\tag{13}
$$

The inset also indicates that the resistive sheet is sandwiched between a dielectric substrate and air. Since both layers are homogeneous, their corresponding eigen-matrices $\mathbb{Q}_i$ (i = 1 or 2)

#198658 - $15.00 USD Received 1 Oct 2013; revised 12 Dec 2013; accepted 12 Dec 2013; published 23 Dec 2013

in (11) are identity matrices with ones in the main diagonal and zeros elsewhere. In particular, the characteristic of homogeneous dielectric layer is described in $\mathbb{Y}_i$, which is a diagonal admittance matrix with $\omega\varepsilon_0\varepsilon_r^{(i)}/k_{zn}^{(i)}$ (i = 1 or 2) on the n^{th} entry.

The SWRG demonstrated in this paper is a single-layered subwavelength grating where the grating bars are composed of thicknessless resistive sheets. A dielectric substrate with perfect electric conductor (PEC) is laid adjacent to the resistive grating, as shown in Fig. 3. The refractive index of the substrate is 1.517. There are many factors that influence the complex reflection coefficient of the resistive grating, for example, the thickness of substrate, the surface resistance of absorbing sheet, and the period and duty cycle of each unit cell. Continuously varying the height of substrate requires laser cutting technique in microwave region. It raises the cost of manufacturing and mass production, and therefore is not favorable. To accomplish an entirely planar design, the thickness of substrate is fixed at 5 mm corresponding to about one quarter wavelength. Besides, the practical fabrication process can be simplified by keeping the surface resistances of every grating sheet the same, while 175 Ω/square is adopted for a 99 % power absorption in this research. For non-periodic configuration of the SWRG, each unit cell has different grating period and duty cycle. Since the whole structure is under normal incidence, the arrangement of SWRG also exhibits symmetric property.

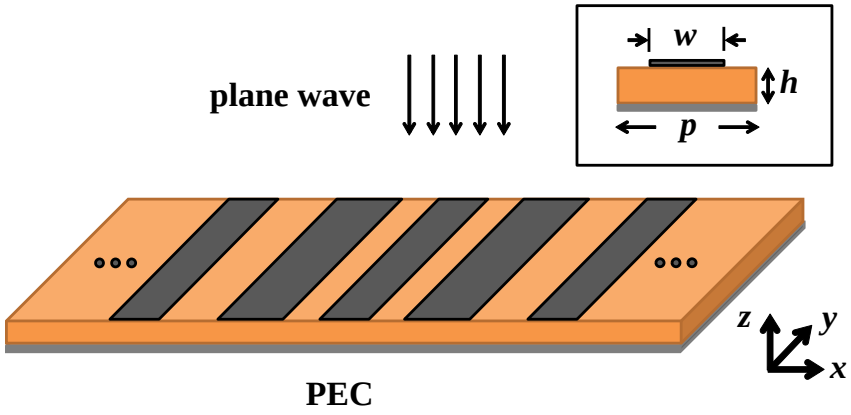

Fig. 3. Schematic plot of the proposed subwavelength resistive grating (SWRG). The refractive index of the substrate (orange) is 1.517. Non-periodic resistive sheets are symmetrically distributed on the dielectric surface.

When the SWRG is illuminated by a normally incident plane wave, the non-periodic surface creates a predetermined phase profile for the reflected wave, which results from the lateral variation of each distinct unit cell along the x-axis. The reflected field is focused given that the phase distribution of the grating component is properly designed. It is well-known that hyperbolic phase response gives rise to a focused reflected beam.

$$\varphi(x) = k_0(\sqrt{x^2 + f_x^2} - f_x) + \varphi_0 \tag{14}$$

where f_x is the focal length, $k_0 = 2\pi/\lambda_0$ and λ_0 is the free-space wavelength. The value of φ_0 can be arbitrary in the current design. Due to the phase compensation for the path from each resistive unit to the focus, the hyperbolic function is chosen as the phase profile which is illustrated in the inset of Fig. 4.

From the above equation we can obtain the reflected phase of each unit cell, as shown in Fig. 4. We intend to use the discretized phase samples to approximate the ideal phase distribu-

#198658 - $15.00 USD Received 1 Oct 2013; revised 12 Dec 2013; accepted 12 Dec 2013; published 23 Dec 2013

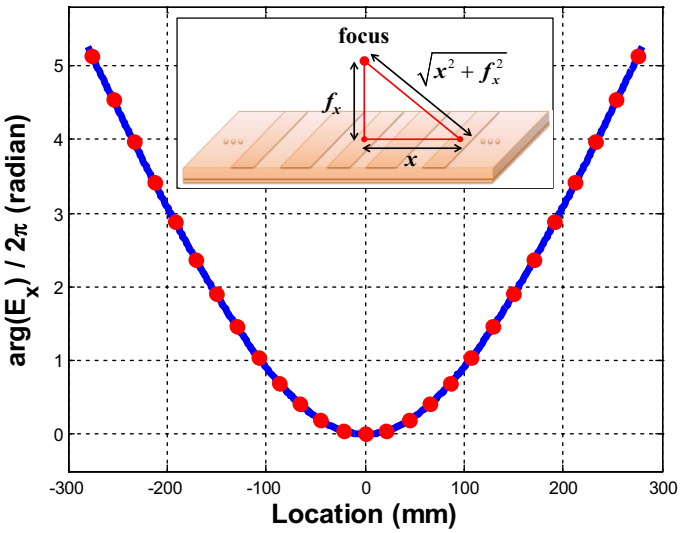

Fig. 4. The phase distribution 1 mm above the non-periodic grating as a function of position. Blue curve represents the ideal phase distribution, while the red circles are the discretized phase samples used to determine the size of each unit cell. The blue curve is derived by setting λ_0 = 30 mm, f_x = 170 mm, and φ_0 = 0 in (14), and a factor of 2π is divided for normalization.

tion. The red circles indicate the required phases, which can be provided by the resistive grating with specific period and duty cycle through careful implementation, and feature a 10π phase shift from edge to center. Additionally, the reflection magnitude of each unit cell should not exceed 0.01, or the absorptivity will be reduced otherwise.

4. Design procedure

In this section, we will explain the design process of the non-periodic SWRG to imprint the specific phase profile $\varphi(x)$ on the reflected wave. To design the SWRG with focusing ability, the first step is to decide the focal length, which is 170 mm in this paper, and obtain the corresponding phase distribution. The second step is to establish the mapping correspondence of geometric parameters (i.e., period and duty cycle) and reflection coefficient, which can be calculated using rigorous coupled wave analysis (RCWA) mentioned in Sec. 2. Although the formulation is for a general two-dimensional case, it can be readily simplified for application to a one-dimensional problem. Structure in Fig. 2 transforms into the inset in Fig. 3 by shorting port 1 and assigning the dielectric substrate and air to medium 1 and 2, respectively. Since a PEC is placed at port 1, the complex reflection coefficient seen from port 2 is given by

$$\mathbb{R} = \mathbb{S}_{22} - \mathbb{S}_{21}(\mathbb{I} + \mathbb{S}_{11})^{-1}\mathbb{S}_{12} \tag{15}$$

The period and duty cycle (defined as the ratio of the sheet width to the period, as shown in the inset of Fig. 3) of a given periodic grating will determine the magnitude and phase of the complex reflectivity for a given wavelength λ_0. Generally, it is convenient to express the results as a look-up table for choosing the adequate distribution of period and duty cycle, as shown in Figs. 5(a) and 5(b). In the calculation domain, the period varies from 5 to 25 mm and duty cycle from 15 to 95 % at the wavelength of 30 mm.

#198658 - $15.00 USD Received 1 Oct 2013; revised 12 Dec 2013; accepted 12 Dec 2013; published 23 Dec 2013

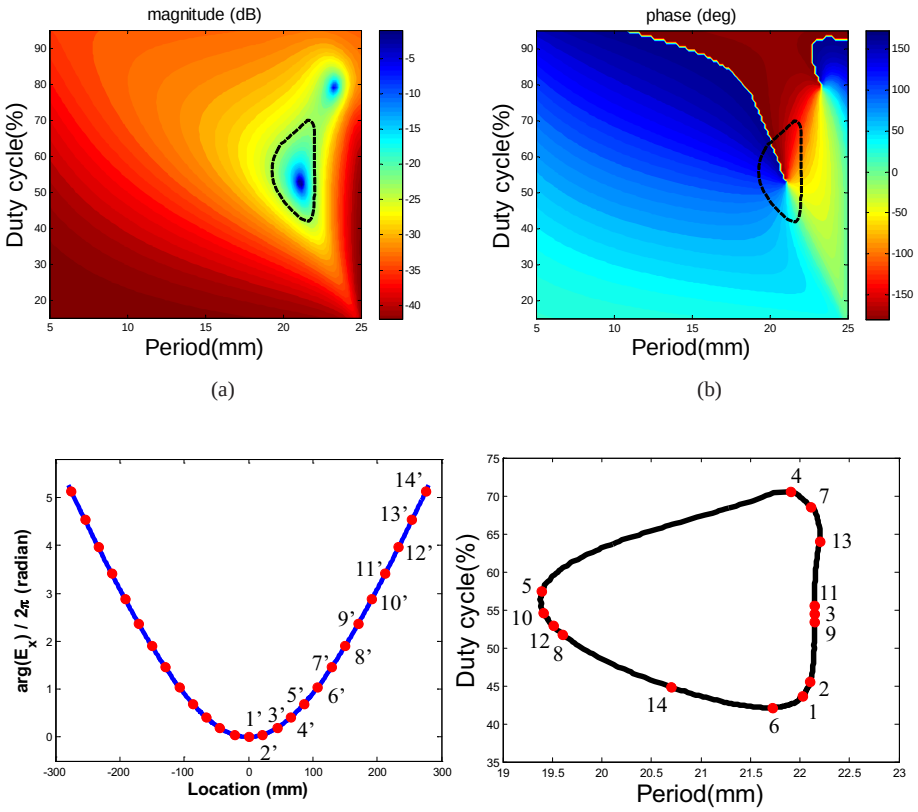

Fig. 5. The contour maps of the magnitude (a) and phase (b) of complex reflectivity, and the locations (c) of discrete phase samples. Magnitude is plotted with logarithmic scale. The black dotted line indicates the path used for actual implementation, where reflectance is kept constant at 0.01 (-20 dB) and maximum phase variation is 2π. Calculation is conducted for R_S = 175 Ω/square, thickness = 5 mm, refractive index = 1.517, wavelength = 30 mm, and incident angle = 0°.

The design freedom is determined by the range of phase variation acquired through dimensional scaling of each resistive grating. By selecting appropriate substrate thickness and surface resistance, a complete phase change modulo 2π can be obtained with high absorptivity. Given the target reflectance of -20 dB, corresponding to a 99 % power absorption, the total phase range of 2π can be realized by varying both period and duty cycle along the dotted path shown in Figs. 5(a) and 5(b). Considering both the phase samples from (14) and the dotted phase path, the actual dimension of the whole SWRG is decided and drawn in Fig. 5(c) through the enumerations with and without prime. Note that only 14 points are considered because of symmetry. As far as the allocation of gratings with various periods is concerned, the discrete algorithm is referred to [28]. TM-polarized wave is assumed in this work, and the design in accordance with TE-polarized wave can be accomplished in the same manner.

#198658 - $15.00 USD Received 1 Oct 2013; revised 12 Dec 2013; accepted 12 Dec 2013; published 23 Dec 2013

5. Simulation results

After the unit cell analysis of periodic SWRG, the numerical simulation is carried out to investigate the characteristic of the final design. Here we used the finite integration technique (FIT), the time domain solver of CST Microwave Studio, to simulate a one-dimensional non-periodic SWRG with focusing ability, which has a diameter of 572.17 mm and a focal length of 170 mm. The quantity 572.17 mm comes from the summation of the periods from 27 unit cells.

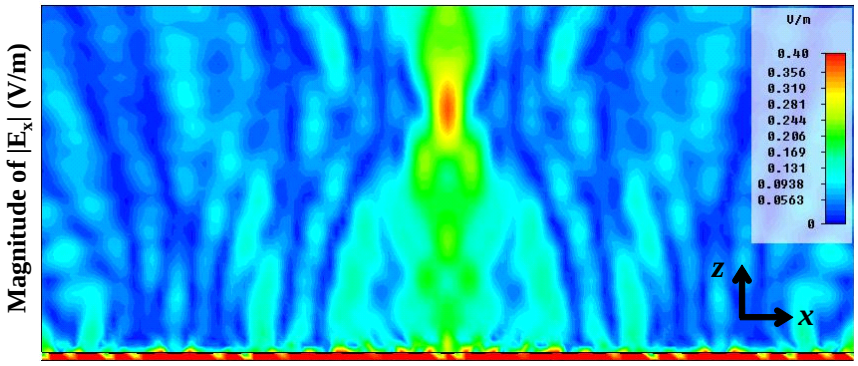

Fig. 6. Reflected electric field distribution as a function of position under normal incidence of plane wave. The field on the transmission side is ignored. Incident electric field has a magnitude of 1 V/m.

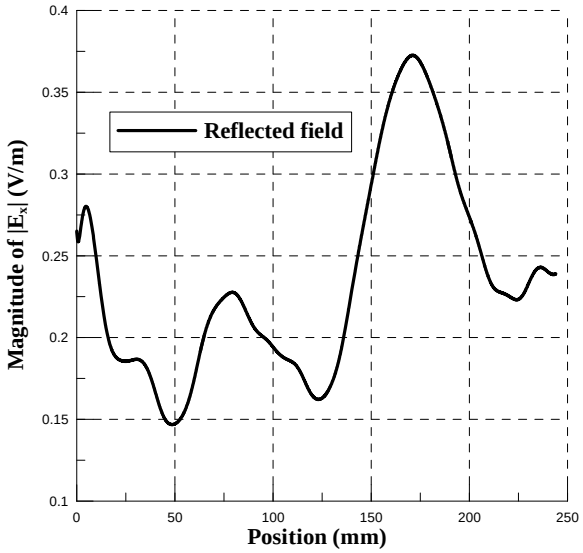

Fig. 7. Reflected electric field distribution along *z*-axis at the center of grating. Calculated focal point is at z = 172 mm.

When the lens is very long and contains multiple resistive units, such a configuration is referred to as an array. For an equally spaced linear array, the side lobe level decreases while increasing the number of elements. The side lobe level can be further reduced using Dolph-Chebyshev method or Taylor line source method in the aspect of antenna design, if the number of elements is sufficient. Although we care more about the main lobe for the lossy lens, adding

#198658 - $15.00 USD Received 1 Oct 2013; revised 12 Dec 2013; accepted 12 Dec 2013; published 23 Dec 2013

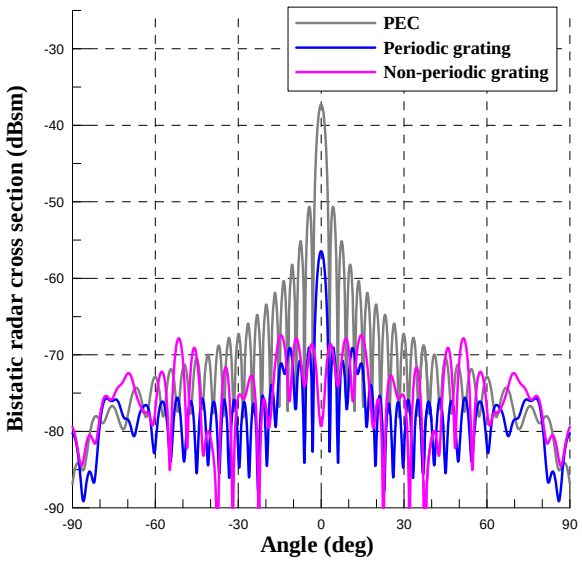

Fig. 8. Radar cross section (RCS) of bistatic scattering in the positive z half-plane. Three kinds of structures having the same width of 572.17 mm are compared. For the periodic grating (blue curve), the period is 21.1914 mm, and duty cycle is 0.4301.

extra resistive units, which also brings the dimension larger, is advantageous to the side lobe suppression and RCS reduction.

The performance of the non-periodic SWRG is analyzed in a TM-polarization environment, and a normally incident plane wave at a wavelength of 30 mm illuminates the whole structure. The reflected E-field intensity is plotted in Fig. 6. When the incident plane wave propagates along the $-z$ direction, the scattered field is mostly focused to a spot 172 mm (shown in Fig. 7) above the grating, which is of little deviation from 170 mm. The NA is 0.857. Subtraction of the incident field from total field is implemented to obtain the field distribution.

Although the near-field property is discussed above, the main purpose of this research is to improve the radar cross section (RCS) reduction by the non-periodic design. Distinct from the dielectric subwavelength grating (SWG) or high contrast grating (HCG) having optical functionalities in the near-field region [28, 29], the proposed resistive grating absorbs the incoming energy by the resistive sheet and lowers the re-radiated power in the far-field region. The reason why making a focusing absorber is due to the fact that the far-field pattern can be converted directly from near-field through Fourier transformation. When the scattered wave is focused on a spot in the near-field region, the radiated energy in far-field will not concentrate in a particular direction unless it's a Gaussian distribution.

To compare the performance of the non-periodic grating to a periodic one under the same criterion, both of them must have the same size and absorptivity. Consequently, the period is derived directly after dividing the total length 572.17 mm by 27, which gives 21.1914 mm. Then considering the plot on the right-hand side of Fig. 5(c), a straight line x = 21.1914 and the route locus will give two intersection points. Although either can fit in with our demand, the duty cycle 0.4301 is chosen for computation. Furthermore, an equally wide PEC plate is also considered for reference. The curves of bistatic RCS in agreement with three cases are illustrated in Fig. 8. We can observe that the periodic SWRG gives a 19.16 dB reduction in RCS to the pure PEC plate in the boresight direction ($\theta = 0^\circ$), which is close to the designated value of 20 dB. However, the radiation pattern of the periodic resistive grating (blue curve) becomes

#198658 - $15.00 USD Received 1 Oct 2013; revised 12 Dec 2013; accepted 12 Dec 2013; published 23 Dec 2013

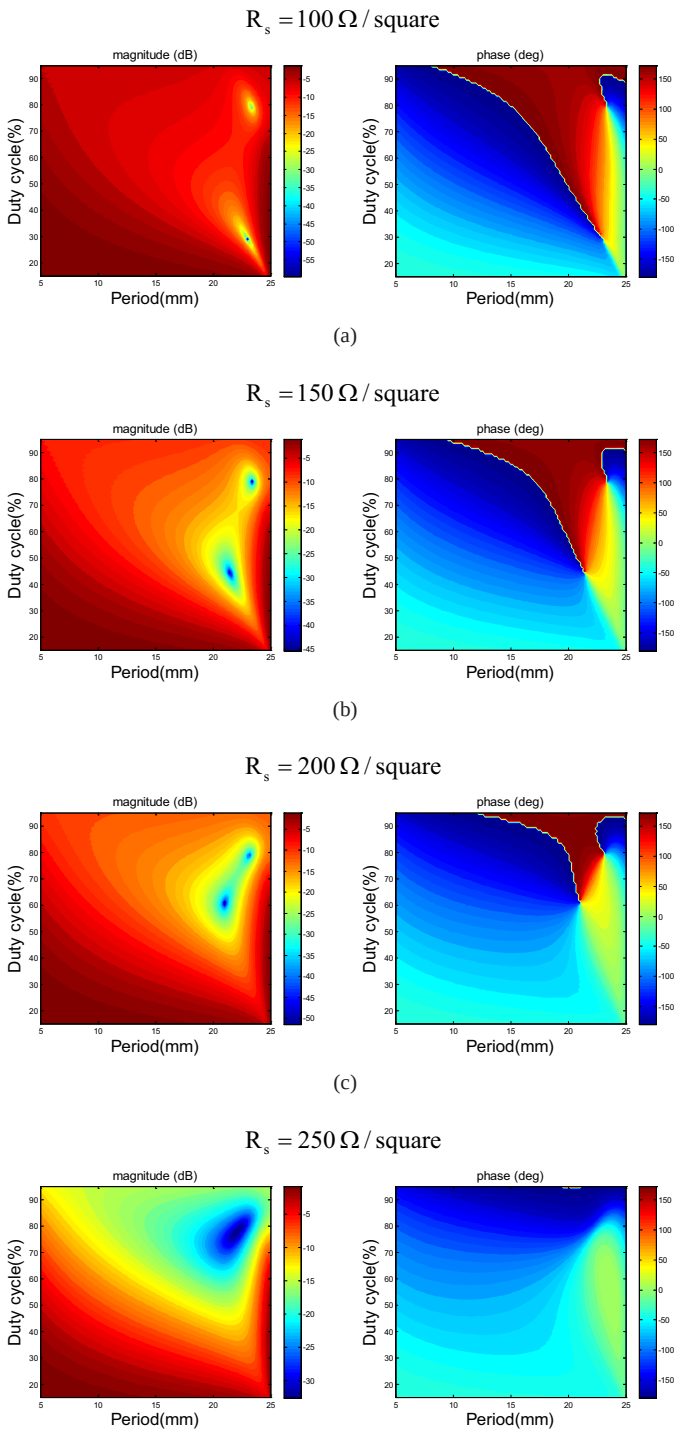

Fig. 9. Various contour maps by calculating the complex reflection coefficients for different surface resistance. (a) R_S = 100 Ω/square, (b) R_S = 150 Ω/square, (c) R_S = 200 Ω/square, (d) R_S = 250 Ω/square.

#198658 - $15.00 USD Received 1 Oct 2013; revised 12 Dec 2013; accepted 12 Dec 2013; published 23 Dec 2013

directional in virtue of the consistent phase front. In the case of non-periodic design, the value of main beam at $\theta = 0^\circ$ drastically drops another 22.86 dB, and the pattern (pink curve) is reshaped with higher uniformity, which confirms the efficacy of this work. Specifically, the maximum radiation pattern of non-periodic design is superior to periodic one by 10.99 dB over the specular angular region. Although the total absorbed powers of the two gratings are similar, the presented non-periodic SWRG possesses less visibility in microwave regime. In practice, the graphene strips are known to behave as resistive strips with frequency-dependent resistivity. Since our goal is to establish the design procedure of non-periodic SWRG, the experimental verification is considered as a future work, which is not included in this paper.

6. Discussion

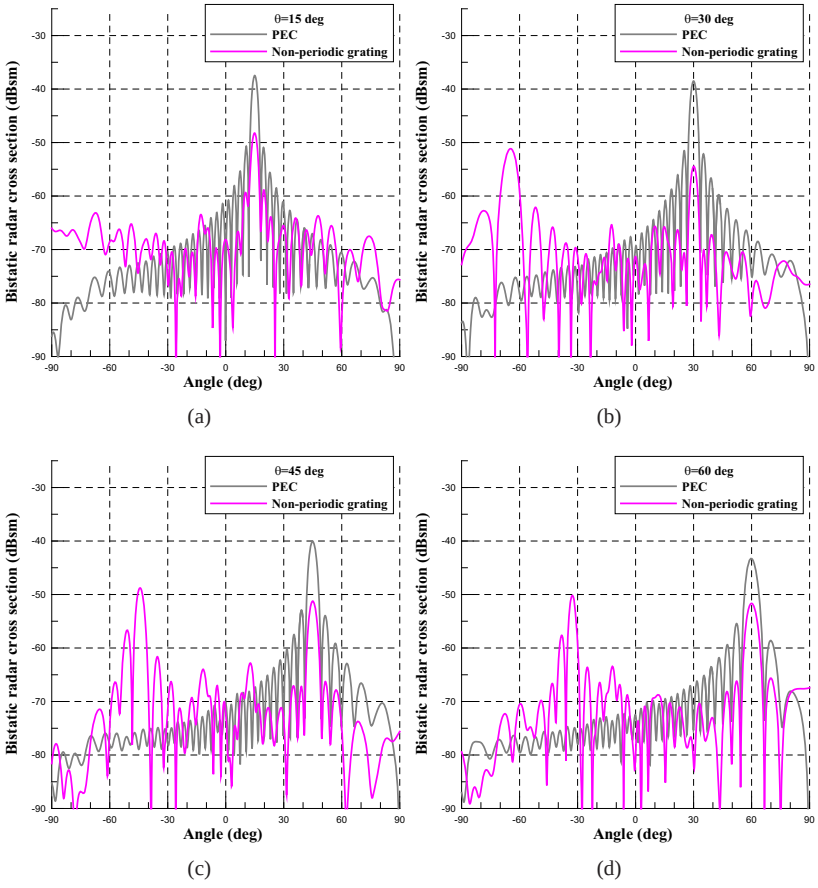

Fig. 10. Bistatic radar cross sections for the proposed non-periodic SWRG and PEC plate under several incidence angles. (a) $\theta = 15^\circ$, (b) $\theta = 30^\circ$, (c) $\theta = 45^\circ$, (d) $\theta = 60^\circ$.

Detailed discussions of few technical points raised in the main text are provided in this section. First, the relationship between sheet resistance and RCS reduction is investigated. Setting the resistance from 100 to 250 Ω/square with a step of 50 Ω/square, four groups of contour maps are obtained using the proposed RCWA method, and the colors represent the complex reflectivity. We attempt to seek a route that remains constant in the magnitude map and involves a complete 2π variation in the phase map simultaneously, which is actually a closed path surrounding either

#198658 - $15.00 USD Received 1 Oct 2013; revised 12 Dec 2013; accepted 12 Dec 2013; published 23 Dec 2013

a single or multiple branch points. In Fig. 9, when R_s = 100, 150, and 200 Ω/square, two branch points can be observed clearly from the maps, but there are no branch points in Fig. 9(d). These plots give us the information that reveals the possible range of desired surface resistance.

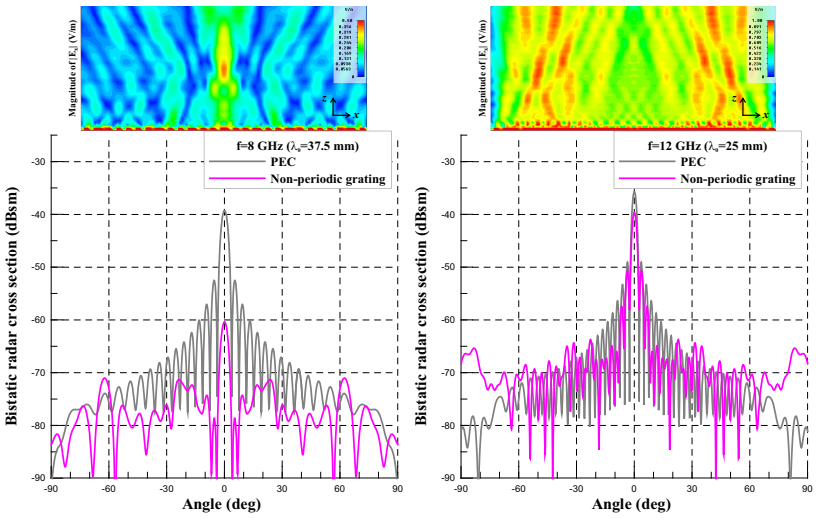

(a) (b)

Fig. 11. Bistatic radar cross sections for the proposed non-periodic SWRG and PEC plate at different operation frequencies. (a) 8 GHz, (b) 12 GHz.

Second, the angular dependence and bandwidth of the proposed structure are discussed. Bistatic RCS of the proposed structure and a reference metallic plate of the same size are compared under oblique incidence. The incidence angle of incoming plane wave is taken from -15° to -60° with a decrement of 15° at 10 GHz (λ_0 = 30 mm). Figure 10 shows that, both structures generate main beams at the specular reflection direction, and the SWRG reduces the main lobe level with a degraded performance. With regard to the bandwidth, the near-field distribution and far-field RCS under normal incidence are studied at 8 and 12 GHz (λ_0 = 37.5 and 25 mm), respectively. As shown in Fig. 11, a focusing spot appears at 8 GHz, which results in a far-field pattern with moderate uniformity. However, the functionality of SWRG nearly vanishes at 12 GHz, which makes the far-field behavior of the grating nothing but a PEC plate.

In the current prototype, there are totally 27 unit cells having 14 different sets of grating periods and duty cycles due to symmetry. These resistive elements possess hyperbolic phase response and identical absorptivity only at a single frequency under particular incidence angle ($\theta = 0^\circ$). Therefore, when the operation condition changes, the focusing ability disappears accompanying poor RCS reduction.

7. Conclusion

We have demonstrated a planar focusing reflector with high absorptivity employing non-periodic SWRG design. Desired phase profile can be imprinted on the constituting unit cell by altering the period and duty cycle. The full-wave simulation reveals the focusing phenomenon with an NA of 0.857. Specifically, the far-field RCS reduction benefits from the near-field focusing feature and can be enhanced 22.86 dB at main beam and 10.99 dB over the entire specular area comparing to periodic SWRG. Furthermore, such structure is simple to fabricate with silk screen process printing and can be readily integrated into stealth technology, aerospace engi-

#198658 - $15.00 USD Received 1 Oct 2013; revised 12 Dec 2013; accepted 12 Dec 2013; published 23 Dec 2013

neering, and microwave anechoic chamber.

Acknowledgment

The corresponding author of this paper would like to acknowledge CST™ for their support in providing software for numerical simulation.

#198658 - $15.00 USD Received 1 Oct 2013; revised 12 Dec 2013; accepted 12 Dec 2013; published 23 Dec 2013